Probing the Effect of Gaseous Hydrocarbon Precursors on the Adsorptive Efficiency of Synthesized Carbon-Based Nanomaterials

Haiyam Mohammed Alayan[1,*], Mustafa Mohammed Aljumaily[2],
Mohammed Abdulhakim Alsaadi[3], and Mohd Ali Hashim[4]
[1] Chemical Engineering Department, University of Technology, Baghdad, Iraq
[2] Department of Civil Engineering, Al-Maaref University College, Ramadi, Iraq
[3] National Chair of Materials Sciences and Metallurgy,
University of Nizwa, Nizwa, Sultanate of Oman
[4] Chemical Engineering Department, University of Malaya, Kuala Lumpur, Malaysia

ABSTRACT: The present work investigates the effect of the type of carbon precursor on the adsorptive proficiency of as-prepared carbon nanomaterials (CNMs) for the removal of methylene blue dye (MB) from aqueous media. A comparison study was applied to assess the growth of CNMs from the decomposition of methane (CNMY1) and acetylene (CNMY2) using response surface methodology with central composite design (RSM/CCD). The produced nanomaterials were characterized using FESEM, EDX, TEM, BET surface area, Raman, TGA, FTIR, and zeta potential. The as-prepared adsorbent displayed different morphologies and under the experimental conditions, 10 mg of CNMY1 and CNMY2 was responsible for 97.7 % and 96.80% removal of dye. The maximum adsorptive uptake predicted by Langmuir isotherm was about 250 and 174 mg/g for CNMY1 and CNMY2, respectively. The as-synthesized carbon nanomaterial in this study could be explored as a great potential candidate for dye-bearing wastewater treatment.

Keywords: Adsorption; Carbon nanomaterials; Chemical vapor deposition; Dyes; Response surface methodology**.**

التحقق من تأثير السلائف الهيدروكربونية الغازية على الكفاءة الإدمصاصية للمواد النانوية المستخلصة من الكربون

هيام محمد عليان *، مصطفى محمد الجميلي، محمد عبدالحكيم السعدي و محمد علي هاشم

الملخص: في هذه الورقة البحثية، تم تصنيع انابيب الكربون النانوية من نوعين مختلفين من الغازات الهيدركربونية (الميثان والاستيلين) بواسطة مفاعل كيميائي تحليلي تبخيري وعامل مساعد ثابت. وقد استخدم البرنامج الحاسوبي Design Experiment لتصميم مخطط التجارب المختبرية للحصول على أفضل قيمة لكل واحدة من عوامل التفاعل والتي تتضمن درجة حرارة التفاعل، زمن التفاعل، ونسبة خلط الغازات المستعملة على ان تتحقق في المنتوج أفضل كمية نمو مع افضل قدرة على ازالة صبغة الميثيل الازرق من الماء. لقد فحصت خواص المادة الناتجة باستخدام FEESM، EDX ، TEM، BET، واجريت فحوصات الاشعة تحت الحمراء بFTIR، والسلوك الحراري باستخدام TGA، وجهد الزيتا Zeta potential. بينت النتائج ان 10 ملغرام من المادة الممتزة الناتجة من تفكك الميثان والاستلين لها القدرة على ازالة الملوث بنسبة 79.7 و96.8 % على الترتيب. ووجد ان الايزوثرم حسب Langmuir خير ما يمثل النظام وبامتصاصية قصوى تصل الى 250 و174 ملغم/غم للمادة المنتجة من تفكك الميثان والاستلين عل الترتيب. بينت الدراسة ان المادة االنانوية التي تم تصنيعها قد ابدت أداءا متميزا في الامتزاز مما يجعلها مادة واعدة لاستخدامها لأغراض الامتزاز المتنوعة.

الكلمات المفتاحية: الامتزاز؛ انابيب كاربونية نانوية؛ مفاعل تبخيري ذو عامل مساعد؛ الاصباغ الملوثة.

*Corresponding author's e-mail: hayomchm@yahoo.com

DOI:10.24200/tjer.vol17iss1pp47-58

1. INTRODUCTION

Carbon nanomaterials (CNMs) have been intensively investigated for environmental applications due to their outstanding properties. They have enlightened different prospects as attractive sorbents for the removal of undesirable pollutants from water. Their high surface area, hybridized sp^2 carbon cluster and optimal binding efficiency enable strong adsorption capacity for organic contaminants (Hu *et al*. 2019; Sun *et al*. 2016).

Among the various techniques being used to synthesize CNMs, the chemical vapor deposition (CVD) is considered as the most promising technique, due to its versatility and suitability for large scale production. In CVD process and under tunable growth conditions, a statistical study should be conducted to achieve an adequate evaluation of the optimal growth conditions for CNMs, such as the utilized catalyst, carbon precursor type and flow rate, growth temperature and reaction time (Alayan *et al*. 2019; Gromov *et al*. 2016).

The agglomeration and ineffective recovery of CNMs are considered significant limitations which will confine their application in environmental remediation. Thus, it is essential to develop innovative adsorbents that can overcome the current challenges. Possible techniques proposed to resolve these drawbacks include centrifugation and attachment of magnetic nanoparticles. Nevertheless, both options will crucially add cost and complexity to the adsorption process. Accordingly, it is believed that growing carbon nanostructures on micro-scaled carbon support will enlighten the production of promising alternatives to the conventional adsorbents (Meshot *et al*. 2017).

Industrial effluents accept worrying quantities of colored pigments which impose harmful effects on the human health and surrounding ecosystems. Methylene blue (MB) contaminant has a potential danger of bioaccumulation due to its stability and low biodegradability, hence, efficient removal techniques of practical significance is imperative to remove it from industrial wastewaters before it is released to the environment. Of all treatment methods, adsorption based process has been widely implemented since it is simple, bear large volume of wastewater and devoid of utilizing organic solvents (Elsagh *et al*. 2017; Siddiqui *et al*. 2019).

In this work, we aim to assess the effect of hydrocarbon source being supplied in CVD reactor on the adsorption capacity of the as-prepared CNMs. Unlike previous studies that usually employ metallic substrates in the growth process of CNMs we fabricated our carbon nanomaterial by incorporating powder activated carbon (PAC) as analogues of non-carbon supports to boost the synergetic effect of hybridized CNMs to enhance their adsorptive affinity (Alayan *et al*. 2017). In this context, PAC was employed as a catalyst substrate to motivate the growth of CNMs from methane and acetylene decomposition. Response surface methodology with central composite design (RSM-CCD) technique was applied to optimize the preparation parameters followed by characterizing the as-prepared nanomaterial using EDX, BET, FESEM, TEM, Raman spectroscopy, TGA, FTIR, zeta potential and Goniometer. Later, the adsorption performance of the fabricated hierarchical CNMs was investigated for the removal of MB dye from water samples.

2. MATERIALS AND METHODS

2.1 Materials

Methylene blue, powder activated carbon, nickel (II) nitrate hexahydrate Ni $(NO_3)_2{\cdot}6H_2O$, were purchased from Sigma-Aldrich. Methane CH_4, acetylene C_2H_2, hydrogen H_2, nitrogen (N_2), were supplied in analytical grade and used without further purification.

2.2 Synthesis of CNM/PAC using CVD

A mixture of 2 g of dried PAC and 5 mL catalyst solution of nickel (II) nitrate hexahydrate (1.0 wt %) was sonicated at 60ºC for 1 h. Then the Ni-impregnated PAC was dried at 100ºC overnight. The dried and grinded Ni/PAC samples were exposed to two sequenced stages of thermal treatment in CVD reactor including calcination and reduction at 350 and 600 ºC for 2 and 1 h under 200 mL/min of N_2 and H_2. The growth of hierarchal CNM/PAC was achieved by shuffling a ceramic boat of the Ni/PAC into the reaction tube of CVD reactor. The growth process was conducted with the following conditions: CH_4 and H_2 were introduced to the CVD reactor at a ratio range of 1-4 within a temperature range of 750-1000 ºC for 20 -60 min. Then the reactor was cooled and the produced CNMs were collected. The second hierarchal CNM/PAC was synthesized from the decomposition of C_2H_2 following the same experimental procedure. However, in this case the growth reaction was conducted within the temperature range 550-750ºC. The yield of CNMs (CNMY) was calculated using equation (1):

$$\text{Yield} = \frac{M_2 - M_1}{M_1} \quad (1)$$

where M_2 and M_1 are the weight of the sample after and before reaction, respectively.

2.3 Experimental Design and Optimization

A design of experiment using CCD was employed to investigate how to obtain optimal growth parameters namely, hydrothermal temperature, reaction time and input gas ratio. The suggested regression model and the relevant statistical parameters were evaluated by the analysis of variance

(ANOVA). Additionally, for optimization sake, maximizing the growth of CNMs was our response criterion. Accordingly, tridimensional plots were constructed to demonstrate the interaction between the underworking growth parameters.

2.4 Characterization

The PAC, Ni/PAC, and CNMs were dispersed onto copper grids to examine their surface morphologies using SEM equipped with Energy Dispersive X-Ray Spectroscopy and Transmission Electron Microscopy. Raman spectra and thermo-gravimetric analysis of CNMs were developed. The BET method was carried out to determine the surface area of the prepared nanomaterials. The FTIR spectra over the range 4000 to 400 cm^{-1} was used to analyze the surface changes. Surface charge analysis was investigated using the zeta potential measurements of a 0.01 wt % suspensions by Zetasizer. Finally, to debate the hydrophobicity issue, the goniometer was used to assess the surface hydrophobicity in terms of its contact angle.

2.5 Measurements of Dye Performance

The removal of MB on the as-prepared CNMs produced from the decomposition of CH_4 and C_2H_2 were carried in a batch mode as follow: a fixed amount of each adsorbent (10 mg) was agitated for 30 min at room temperature into the dye solution (50 ml) at initial concentration of 50 mg/L and pH 11. At the end of the adsorption experiments, the dye solution was centrifuged and the persisted concentration was determined using UV-vis spectroscopic at maximum wavelength (665 nm). The removal efficiency and the adsorbent uptake (mg/g) were calculated by the following relationships:

$$\text{Removal Efficiency (\%)} = \frac{C_o - C_e}{C_o} \times 100 \quad (2)$$

$$\text{Uptake} = \frac{C_o - C_e}{W} \times V \quad (3)$$

where Co and Ce (mg /l) are the initial and equilibrium dye concentrations, respectively, V (L) is the volume the dye solution and W (g) is the amount of the adsorbent. The adsorption efficiency can be demonstrated via the analysis of experimental data to estimate the best fitted kinetic models and adsorption isotherms (Chen and Bai 2013). Kinetics of adsorption of MB on as-prepared CNM were investigated using both the pseudo-first-order and pseudo-second-order models. In addition, Langmuir and Freundlich isotherms were applied to study the sorbent-sorbate interactions.

3. RESULTS AND DISCUSSION

3.1 Model Establishment and Statistical Analysis

The growth temperature (A), growth time (B) and input gases flow ratio; (H_2/CH_4) or (H_2/C_2H_2) (C) were optimized for CNM/PAC synthesis using 2-level CCD with one central point by the RSM/CCD method. The DOE software suggested conditions covered the growth temperature of 750 -1000 ºC, 550 - 750 ºC for CH_4 and C_2H_2 decomposition, respectively. Also, for both hydrocarbon precursor, the reaction time and gases ratio were varied under the range of 20 - 60 min, 1.0 - 4.0. The optimizing criterions were devoted to maximizing the yield percentage of CNMY1 and CNMY2 for CH_4 and C_2H_2, respectively, while the independent parameters were kept in prescribed ranges.

The ANOVA summarized in Table 1 shows that the major determinants for CNMY1 obtained from CH_4 decomposition are the growth temperature (A), the interaction of the growth temperature and the gas ratio (AC) and the second-order effect of growth temperature (B^2). The high model F-value and the low p- values < 0.05 of these confirm their significance effect. The high correlation coefficient R^2 value for CNMY1 and CNMY2 (> 0.98) suggest that the

Table 1. ANOVA results for (CNMY1).

*Source	Sum of Square	*df*	Mean Square	*F*-Value	*p*-value
Model	2.71	10	0.27	210.54	0.0005
A	1.18	1	1.18	914.87	< 0.0001
B	0.074	1	0.074	57.22	0.0048
C	0.068	1	0.068	52.94	0.0054
AB	0.11	1	0.11	84.02	0.0027
AC	0.23	1	0.23	178.35	0.0009
BC	0.0087	1	0.0087	6.76	0.0804
A^2	0.009	1	0.009	69.48	< 0.0036
B^2	0.043	1	0.043	33.05	0.0105
C^2	0.0011	1	0.0011	0.89	0.4158
A^2C	0.048	1	0.048	37.40	0.0088
	R- Squared 0.998			Std.Dev. 0.0359	
	Adj. R-Squared 0.994			C.V. % 1.35	
	Pred. R-Squared 0.938			precision 46.61	

*A (ºC): Temperature, B (min): Time, C (feed gas flow ratio): H_2/CH_4

Table 2. ANOVA results for CNMY2.

Source	Sum of Square	*df*	Mean Square	*F*-Value	*p*-value
Model	0.692	8	0.0865	101	0.00986
A	0.0176	1	0.0176	20.4	0.0456
B	0.0522	1	0.0522	60.8	0.0160
C	0.0334	1	0.0334	38.9	0.0247
AB	0.0654	1	0.0654	76.1	0.0129
AC	0.0921	1	0.0921	107.0	0.00920
BC	0.231	1	0.231	269.0.	0.00370
A2	0.0197	1	0.0197	23.0	0.0409
A2 B	0.0428	1	0.0428	49.9	0.0195
	R- Squared 0.998			Std. Dev.0.0293	
	Adj. R-Squared 0.988			C.V. % 0.604	
	Pred. R-Squared 0.929			precision 26.4	

*A (ºC): Temperature, B (min): Time, C (feed gas flow ratio): H_2/C_2H_2

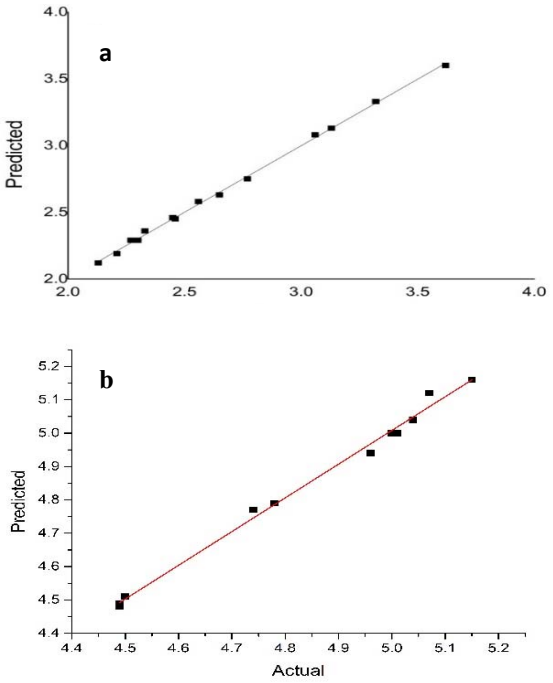

Figure 1. Predicted vs. actual values; (a) CNMY1, (b) CNMY2.

Table 3. The optimum conditions suggested by DOE for CNMY1.

No.	A	B	C	CNMY1%	Desirability	
1	950	60.0	1.00	36.7	0.989	✓
2	950	59.8	1.00	36.5	0.986	
3	950	60.0	1.00	36.5	0.986	
4	950	60.0	1.03	36.4	0.984	
5	950	59.7	1.00	36.3	0.982	
6	950	60.0	1.13	35.7	0.970	
7	950	60.0	1.22	35.1	0.959	
8	950	60.0	1.00	33.4	0.927	
9	950	60.0	1.52	33.0	0.917	
10	950	20.0	1.00	23.0	0.674	

Table 4. The optimum conditions suggested by DOE for CNMY2.

No.	A	B	C	CNMY2 %	Desirability	
1	560	38.0	1.00	154.47	0.919	✓
2	561	38.0	1.00	152.9	0.916	
3	560	38.5	1.00	154.47	0.914	
4	560	38.0	1.12	152.9	0.913	
5	561	38.4	1.00	154.47	0.912	

obtained model offers a successful correlation between the growth variables and good estimation of the responses which is confirmed by the plots of their predicted values against the actual values presented in Fig. 1a and 1b. Furthermore, the statistical results in Table 2 support the significance of the suggested model for CNMY2 from C_2H_2 pyrolysis for the linear terms (A), (B), and (C). The interaction effect of (AC) and (BC) displayed p-values of 0.009 and 0.0036, respectively indicating their strong impact over the studied range as well. The regression equation for CNMY1 and CNMY2 in terms of their actual values are given by equations (4) and (5):

$$Ln\ CNMY1 = -11.4 + 0.0304\ A + 0.0789\ B + 11.0\ C + 5.79 \times 10^{-5}\ AB - 0.0251\ AC - 0.0011\ BC - 1.45 \times 10^{-5} A^2 + 0.00046\ B^2 + 0.0128\ C^2 + 1.41 \times 10^{-5}\ A^2 C \quad (4)$$

$$Ln\ CNMY2 = 26.0\ - 0.0637A - 0.385\ B\ - 0.28\ + 0.00121\ AB\ + 0.000715\ AC\ - 0.00566BC + 4.59 \times 10^{-5} A^2 - 8.96 \times 10^{-7} A^2 B \quad (5)$$

3.1.1 Response Surface Methodology

The effect of the substantial factors and the feature of the obtained response surface in the experiment were examined by using RSM/CCD. The interaction effects of the process parameters on CNMY1 and CNMY2 based on the empirical model were illustrated by RSM plots. Fig. 2 displayed an outstanding increase in CNMY1 with increasing the reaction temperature from 750 to 950°C, implying the favor of high reaction temperature for the growth of CNMs Fig. 2a. There was no significant improvement for CNMY1with the increase in (H2/CH4), since high concentration of H2 will motivate the backward reaction thus reducing the yield of CNMY1 Fig. 2b. Also, the CNMY1 improved with increasing growth time and then dropped as the reaction proceeds Fig. 2c. This decrease in the yield of the CNMs at long reaction period is attributed to the catalyst deactivation due to the formation of amorphous carbon. In Fig. 3a, increasing reaction temperature from 550 to 650°C has a distinguished improvement on the throughput of CNMY2 at fixed H2/C2H2 (1.0) which is in agreement with the role of PAC substrate in minimizing the deactivation of impregnated catalyst even at high growth temperatures (Tao and Crozier 2016). However, an increase in CNMY2 for low reaction temperatures and H2/C2H2 at fixed reaction time is observed in Fig. 3b, and the high temperature accompanying with high gas flow ratio was unfavorable for CNMY2. This might be since the high H2 content will accelerate the reduction of metal oxides which in turn encourages the deposition of pyrolytic carbons on the catalytic sites. Moreover, it can be noticed from Fig. 3c that at short reaction time the yield of CNNMY2 was high and almost the same at H2/C2H2 of 1.0 and 4.0 which indicates the insignificance effect of the gas ratio. This observation motivates the production of CNMs at small reaction periods to get high yield and prevent catalyst deactivation as well (Shen *et al.* 2016).

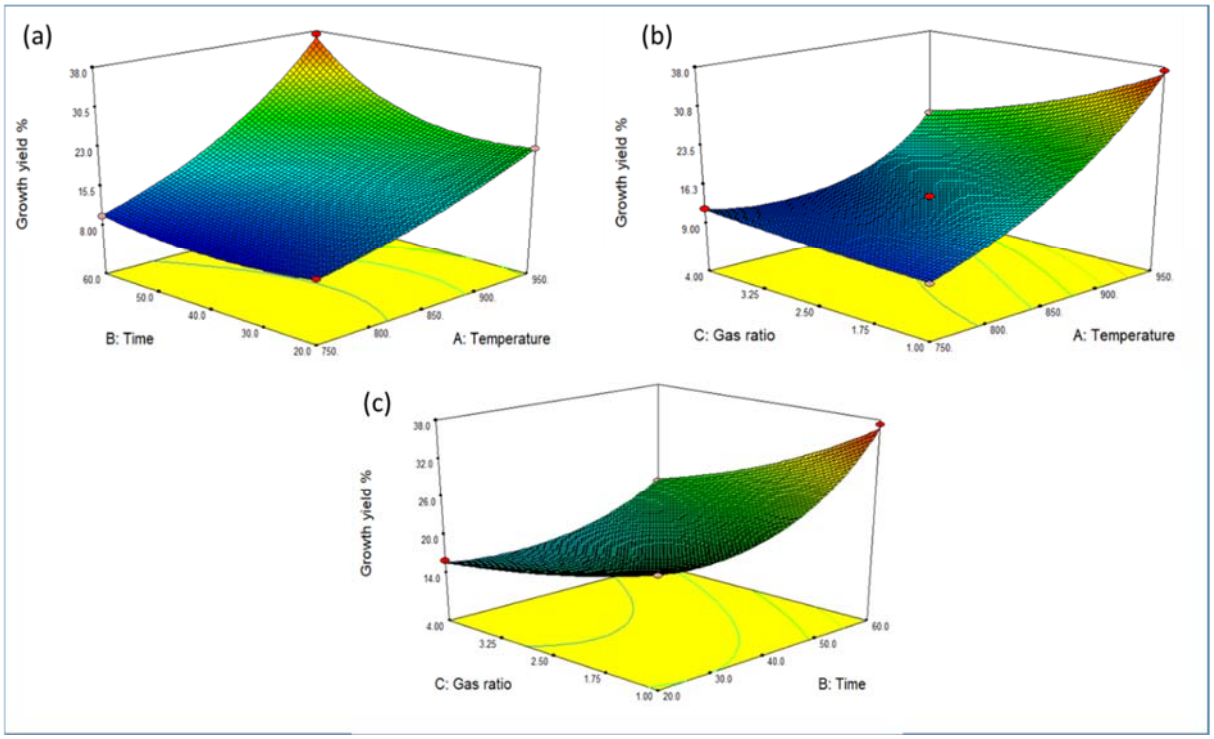

Figure 2. Response surface illustration of the interaction effects on CNMY1: (a) growth temperature and time, (b) growth temperature and gas ratio and (c) time and gas ratio.

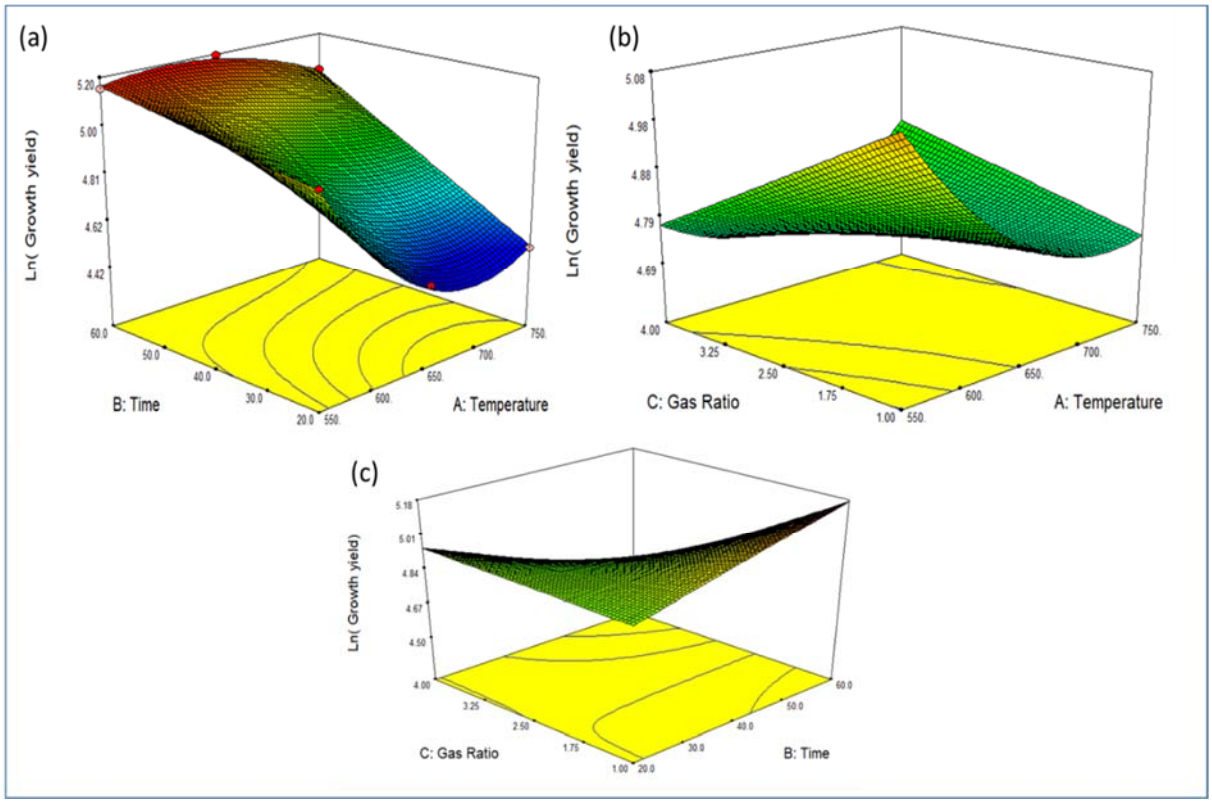

Figure 3. Response surface illustration of interaction effects on CNMY2: (a) growth temperature and time, (b) growth temperature and gas ratio and (c) time and gas ratio.

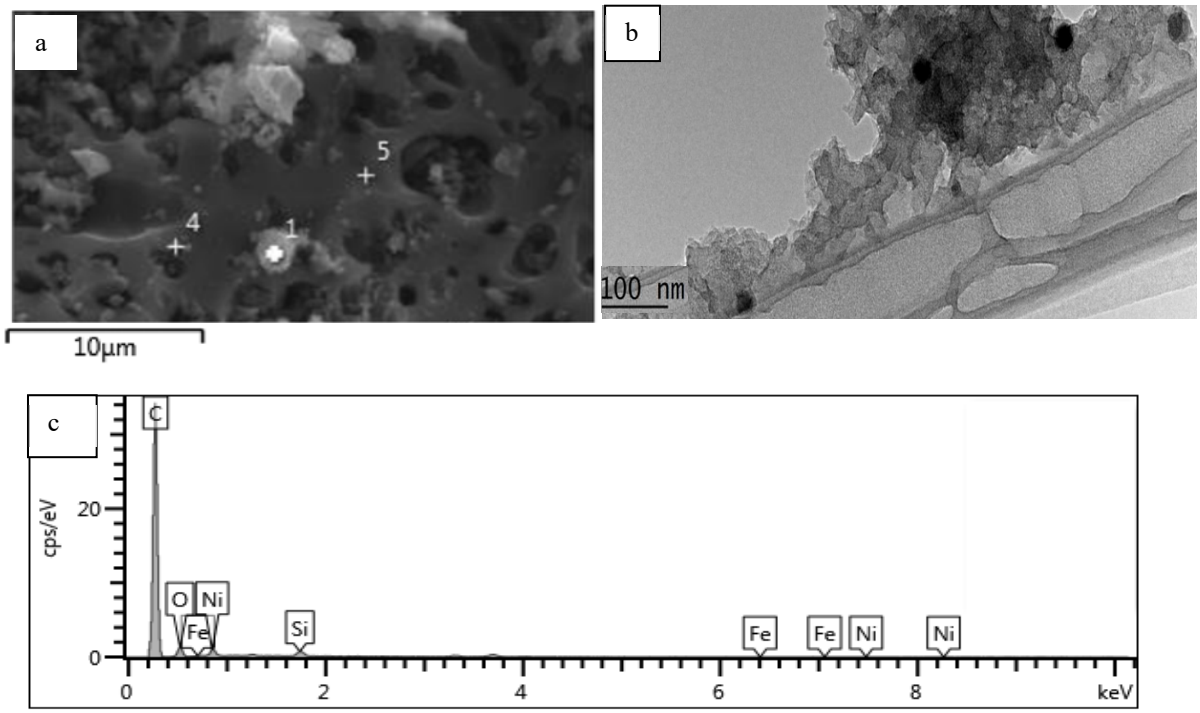

Figure 4. (a) FESEM, (b) TEM and (c) EDX images for Ni/PAC before the growth reaction.

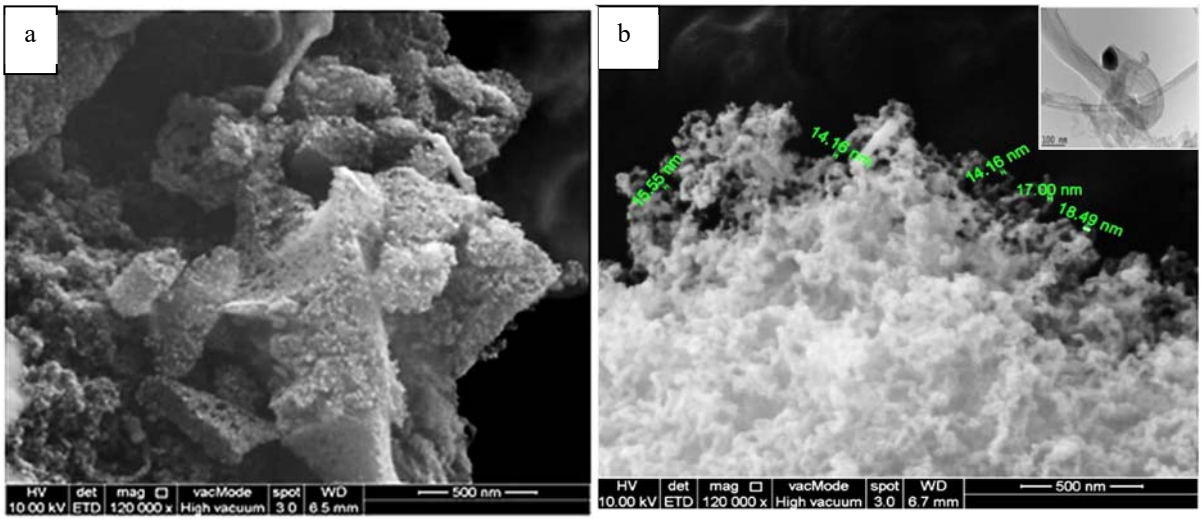

Figure 5. FESEM images of (a) CNMY1 and (b) CNMY2 obtained at optimal conditions.

3.1.2 Optimization Study

Numerical optimization was applied to determine the optimal growth conditions for CH_4 and C_2H_2 decomposition. Thus, the predefined criterions for the optimal working conditions were applied by keeping the synthesis parameters within the prescribed upper and lower limits of the growth conditions in order to achieve the maximum yield and the highest desirability value which will confirm the adequacy of the predicted models. Table 3 indicated that the predicted optimum conditions for CNMY1 were 950°C, 60 min, and 1.0 corresponding to growth temperature, growth time and H_2/CH_4, respectively leading to yield ~ 37.0 %. A yield of ~ 155 % for CNMY2 was obtained at the optimal conditions of a 560°C, 38 min and 1.0 H_2/C_2H_2 (Table 4).

3.2 Characterization

3.2.1 Morphology

The FESEM and TEM images of the nickel-doped activated carbon (Ni/PAC) show a successful imbedding for the catalyst particles in the pores of PAC substrate (Fig. 4a and 4b). The elemental analysis attained from EDX (Fig. 4c) shows that the loaded substrate is comprised of 88.58 wt% carbon, 7.48 wt% oxygen, wt% 3.26 wt% nickel and 0.67 wt% silicon. The growth of various types of CNMs

from this low catalyst amount validates the catalyzing role of PAC and its ability to provide good media for catalyst dispersion (Li *et al.* 2014).

Fig. 5 shows the morphologies of hierarchical nanomaterial shaped from the methane (CNMY1-CH_4) and acetylene (CNMY1-C_2H_2) decomposition at the optimal growth conditions. The hybrid CNMY1-CH_4 displayed in Fig. 5a has groove-like form and resemble the PAC porous structures. CNMY1-CH_4 hybrid is comprised from short interposed carbon nanotubes (CNTs) which are randomly oriented in the substrate matrix and embedded on the solid walls of the pores the activates carbon substrate. The hybrid CNMY1-C_2H_2 in Fig. 5b and 5c, which was obtained at the optimal synthesis conditions, show bushy and graphitized tubular structures of CNTs with 10–40 nm, and an intercalated catalytic nickel nanoparticle (CNP) which was separated from the substrate and confined at the tip of the grown CNT. This observation suggests a tip growth mechanism for the CNT which triggered by the precipitation of the generated carbon fragments on the Ni surface followed by the growth of the tube and terminated finally due to the catalyst deactivation (Jeong *et al.* 2016).

3.2.2 TGA Analysis

The TGA analysis in Fig. 7 assesses the quality and thermal stability of CNMY1 and CNMY2 obtained from CH_4 and C_2H_2. The TGA profile can be highlighted by the initial gradual loss due to moisture evaporation of 2.0 % and 5.0 % followed by constant drops to the onset combustion temperature at 507 and 455 ºC for CNMY1 and CNMY2, respectively. The third region was featured by a steep drop region and ended with the oxidization section of the remaining amorphous carbon at temperature higher than 500 ºC. Additionally, a well-graphitized structure for CNMY1 is obtained and confirmed by its high onset temperature. The TGA analysis indicates that the produced carbon nanostructures from both hydrocarbon precursor sustain a temperature as high as 800 ºC (Zhou *et al*. 2014).

3.2.3 BET Surface Area

The surface area of the PAC, Ni/PAC, CNMY1 and CNMY2 was determined by nitrogen adsorption–desorption measurements. The results illustrated in Table 5 show a reduction in the surface area of Ni/PAC due to the catalyst impregnation. Furthermore, an enhancement in the surface area of the obtained hybrids CNMY1 and CNMY2 because the added structure on the substrate. The total pore volume of CNMY1 and CNMY2 reached 0.29 cm^3/g and 0.44, respectively. This logical result can be ascribed to the development of new micropores resulting from the growth of different nanostructures on the substrate which will be beneficial for improving the adsorbent sorption capacity (Wang *et al*. 2017).

3.2.4 Raman Analysis

Raman analysis displayed in Fig. 7 for the CNMY1 and CNMY2 detected the main D and G characteristic band. The D peak at around 1316 cm^{-1} suggests the presence of disordered graphite structure while the C-C stretching vibration is characterized by the G band at around 1594 cm^{-1}. The high intensity of D band confirms the defective nature of the obtained structure due to the thermal treatment step. Also, the grown hybrids involved multiwall structure confirmed by the disappearance of the radial breathing mode (RBM) at wavelength below 400 cm^{-1}(Ahmad *et al*. 2018). The organizational degree of the obtained hybrids can be represented by I_D/I_G and it is noticed that synthesized nanocarbon structure ratio was 0.9 and 0.82 from the decomposition of CH_4 and C_2H_2, respectively. This indicates that the decomposition of C_2H_2 enhanced the growth of highly graphitized nanostructure which was also observed in the TGA analysis. Also, the CNMs synthesized from acetylene pyrolysis at750°C demonstrated I_D/I_G ratio of 0.74 which suggests a lesser graphitic structure than that obtained at 560°C.

3.2.5 FTIR Analysis

The functional group and surface chemistry of CNMY1 and CNMY2 synthesized at the optimal growth conditions were presented in the FTIR spectroscopy in Fig. 8. Absorption bands at 3450–3500 cm^{-1} assigned to the –OH group. The ascribed peaks from the Ni catalyst carbonyl were found at 1979 and 2138 cm^{-1} (Chavan *et al*. 2012), whereas the peak emerged at ~ 2350 cm^{-1} is attributed to the presence of aromatic sp^2 C–H stretching vibration. The aromatic rings and C=C stretch were appeared at 1447 and 1563 cm^{-1}, respectively. It is observed that the CNMY2 hybrids has fewer functional groups than that produced from CH_4 decomposition, accordingly higher hydrophobicity is expected for CNMY2 (Ezzeddine *et al*. 2016)

3.2.6 Zeta Potential and Contact Angle

The adsorption mechanism is greatly affected by the surface charge and the hydrophobicity of the adsorbent (Aljumaily *et al*. 2018). Ni/PAC is not a hydrophobic material and its cast film a contact angle of 65° as presented in Table 6.

The CNMY1 has lower zeta potential than that obtained for CNMY2.The surface positive charge and basicity of CNMY1 could be due to the oxygen-free carbon sites (π- electron-rich regions) located in the basal planes. Furthermore, the CNMY1 hybrids show enhanced hydrophobicity associated with high contact angle of 138° but lower than that obtained for CNMY2. The super hydrophobic CNMs synthesized from acetylene decomposition demonstrated high contact angle of 160° with high value of zeta potential due to the mutual repulsion of CNMs surface charges.

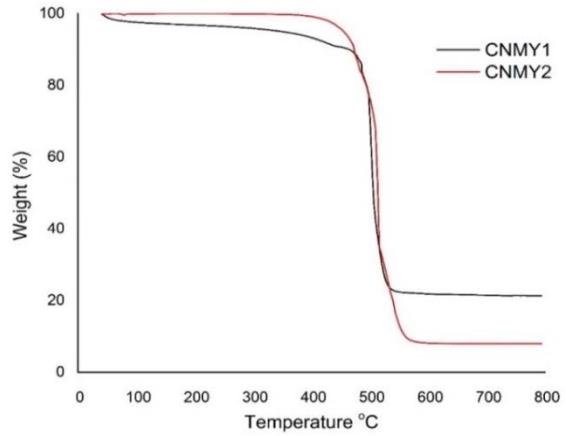

Figure 6. TGA curves for CNMY1 and CNMY2**.**

Table 5. BET results of PAC, Ni/PAC, CNMY1 and CNMY2.

Property	PAC	Ni/PAC	CNMY1	CNMY2
BET (m^2/g)	101.1	97.2	164.6	333.83
Total pore volume (cm^3/g)	0.09	0.07	0.29	0.44
Average pore diameter (ºA)	34.89	21.29	96.19	65.09

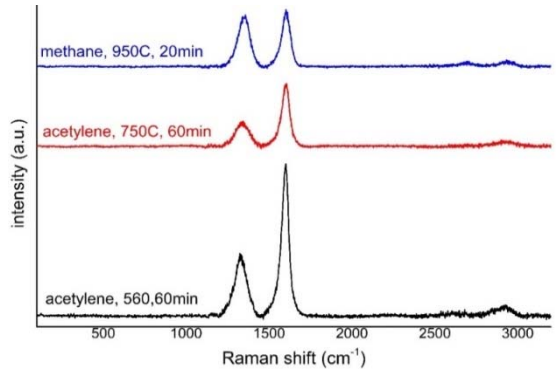

Figure 7. Raman spectrum of CNMY1 and CNMY2.

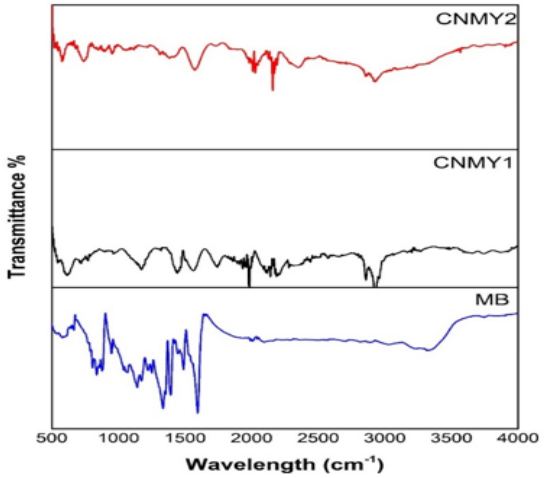

Figure 8. FTIR spectrums for free MB, CNMY1 and CNMY2 after adsorption.

3.2.7 Kinetics and Isotherm Studies

Two models were applied to analyze the kinetic data obtained from the batch experiments of MB adsorption on CNMY1 and CNMY2: pseudo-first order, and pseudo-second models (Fig. 9). The relevant parameters derived from the corresponding equations are provided in Table 7, imply that the adsorption process has not entirely followed the pseudo first-order rate expression for both adsorbents (Fig. 9a and 9b). In contrast, the applicability of the pseudo-second-order model better to describe the sorption kinetics of MB dye is clearly observed in Fig. 9c and 9d confirmed by the high correlation coefficient of the linear plots. This observation suggests the possibility of chemisorption adsorption mechanism through exchange or sharing electrons between the adsorbent and adsorbate (Subramani and Thinakaran 2017). For the isotherm study, the favorability of the Langmuir isotherm can be conveniently represented by the equilibrium parameter (R_L); ($0<R_L<1$) which is defined by equation (6).

$$\mathbf{R_L} = \frac{1}{1 + \mathbf{K_L}\, C_o} \qquad (6)$$

The values summarized in Table 8 and the linear plots presented in Fig. 10 agreed well with the Langmuir isotherm (Model 1) for CNMY1 and CNMY2 signifying monolayer adsorption with heterogeneous surface binding, however, sorption capacity values of CNMY2 was conveniently described by Freundlich model (Model 2) as well. This kind of duality has been stated in many publications (Wang *et al*. 2014). Comparison of the maximum adsorption uptake of MB on several adsorbents are presented in Table 9. The as-prepared hybrid carbon nanomaterials in the present work have demonstrated noteworthy adsorption uptake of 250 and 174 mg/g for CNMY1 and CNMY2, respectively.

Table 6. Zeta potential results for Ni/PAC and the obtained carbon structures.

Sample	Zeta potential (mV)	Contact angle (º)
Ni/PAC	+1.67	65
CNMY1 (950 ºC)	+9.4	138
CNMY2 (560 ºC)	- 34.3	160

Table 7. Experimental values of kinetics model's constants.

Model	Equation	Parameters	Values	
			CNMY1	CNMY2
Pseudo-First-Order	$\ln(q_e - q_t) = lnq_e - K_1 t$	R^2	0.83	0.89
		K_1	0.02	0.03
		q_e	27.0	38.9
Pseudo-Second-Order	$\frac{t}{q_t} = \frac{1}{K_2 q_e^2} + \frac{1}{q_e} t$	R^2	0.999	0.99
		K_1	0.002	0.0015
		q_e	145.0	122.7

Table 8. Linearized equations of studied isotherm models.

Model	Equation	Parameters	Values	
			CNMY1	CNMY2
Langmuir	$\frac{C_e}{q_e} = \frac{1}{K_L\, q_m} + \left(\frac{1}{q_m}\right) C_e$	q_m	250.0	174.0
		K_L	0.65	1.5
		R^2	0.98	0.99
		R_L	0.03	0.01
Freundlich	$lnq_e = lnK_f + \frac{1}{n} lnC_e$	R^2	0.86	0.93
		K_f	85.0	83.7
		n	2.8	2.6

Table 9. maximum adsorption uptake (qm) comparison with previous studies.

Adsorbent	q_m (mg/g)	Reference
CNMY1	250	The present work
CNMY2	174	The present work
MWCNTs	109.31	(Zohre *et al*. 2010)
Activated carbon	123	(Suresh *et al*. 2011)
MWCNTs by CVD (acetylene, Fe/Si)	50.25	(Liu *et al*. 2014)
Cotton stalk	147.06	(Deng *et al*. 2011)
Graphene/magnetite	43.08	(Ai *et al*. 2011)
Oxidized-CNTs	99.83	(Norzilah *et al*. 2011)
Calcined titanate NT	133.33	(Xiong *et al*. 2010)
MWCNTs	59.7	(Wang *et al*. 2012)
Fe_3O_4 – MWCNTs (HNO_3)	48.06	(Ai *et al*. 2011)

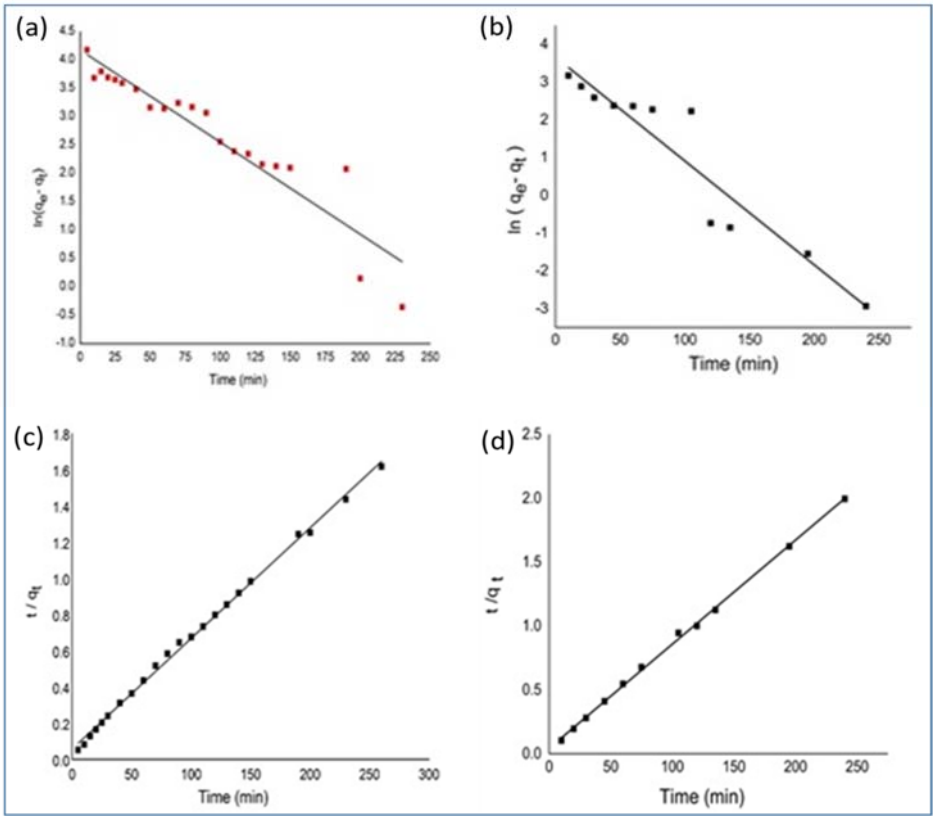

Figure 9. Fittings of Pseudo-first order and Pseudo-second order kinetics models for MB adsorption on CNMY1 (a, b) and CNMY2 (c, d), respectively.

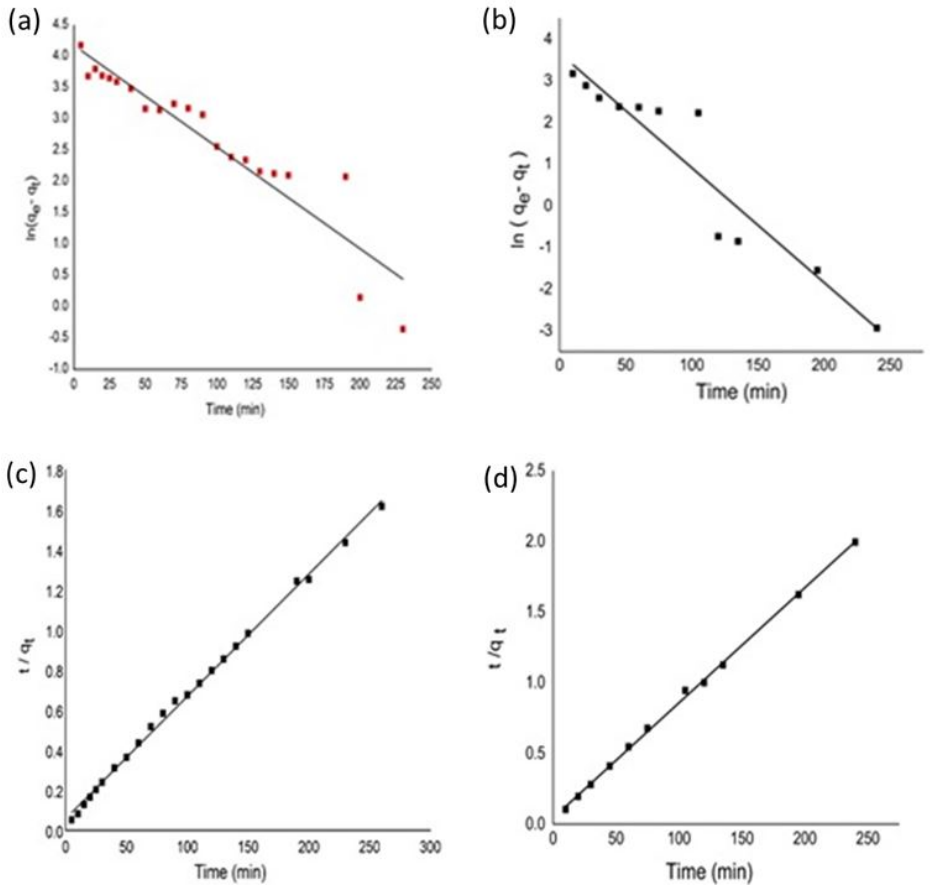

Figure 10. Langmuir and Freundlich model plots for MB adsorption on CNMY1 (a,b) and CNMY2 (c,d), respectively.

4. CONCLUSION

The growth of CNMs from different precursors and optimizing their growth parameters were investigated. The optimal growth conditions for the hybrid carbon nanomaterials obtained from methane and acetylene were found at the temperature of 950, 60, H2/CH4 of 1.0 and 560 ºC, time of 38 min, and H2/C2H2 of 1.0, respectively. Undoubtedly, the carbon source played a significant role to affect the morphology of CNMs deposits due to discrepancies in their pyrolytic behaviors. Methane has the simplest chemical structure and comparatively stable at high-temperature than acetylene. Also, the Gibbs free energies of the C2H2 has lower decomposition temperature than methane which gives rise to lower growth temperature of CNMs. The MB removal process on each adsorbent was fitted well to a pseudo-second order kinetics model and the adsorption system was excellently presented by Langmuir isotherm model with a maximum adsorption capacity of 250 and 174 mg/g for CNM/PAC-CH4 and CNM/PAC-C2H2, respectively.

CONFLICT OF INTEREST

The authors declare no conflicts of interest.

ACKNOWLEDGMENT

The authors would like to acknowledge the University of Malaya Research Grant UMRG (RP034D-15AET) and University of Technology - Iraq for funding this research.

REFERENCES

Ahmad, A., Razali, M. H., Kassim, K., and Amin, K. A. M. (2018). "Synthesis of multiwalled carbon nanotubes supported on M/MCM-41 (M= Ni, Co and Fe) mesoporous catalyst by chemical vapour deposition method." Journal of Porous Materials, 25(2), 433-441.

Ai, L., Zhang, C., and Chen, Z. (2011). "Removal of methylene blue from aqueous solution by a solvothermal-synthesized graphene/magnetite composite." Journal of hazardous materials, 192(3), 1515-1524.

Ai, L., Zhang, C., Liao, F., Wang, Y., Li, M., Meng, L., and Jiang, J. (2011). "Removal of methylene blue from aqueous solution with magnetite loaded multi-wall carbon nanotube: kinetic, isotherm and mechanism analysis." Journal of hazardous materials, 198, 282-290.

Alayan, H. M., Alsaadi, M. A., Abo-Hamad, A., AlOmar, M. K., Aljumaily, M. M., Das, R., and Hashim, M. A. (2017). "Hybridizing carbon nanomaterial with powder activated carbon for an efficient removal of Bisphenol A from water: the optimum growth and adsorption conditions." DESALINATION AND WATER TREATMENT, 95, 128-143.

Alayan, H. M., Alsaadi, M. A., AlOmar, M. K., and Hashim, M. A. (2019). "Growth and optimization of carbon nanotubes in powder activated carbon for an efficient removal of methylene blue from aqueous solution." Environmental technology, 40(18), 2400-2415.

Aljumaily, M. M., Alsaadi, M. A., Das, R., Hamid, S. B. A., Hashim, N. A., AlOmar, M. K., Alayan, H. M., Novikov, M., Alsalhy, Q. F., and Hashim, M. A. (2018). "Optimization of the synthesis of superhydrophobic carbon nanomaterials by chemical vapor deposition." Scientific reports, 8(1), 2778.

Chavan, S., Vitillo, J. G., Larabi, C., Quadrelli, E. A., Dietzel, P. D., and Bordiga, S. (2012). "Functionalization of CPO-27-Ni through metal hexacarbonyls: The role of open Ni2+ sites."Microporous and mesoporous materials, 157, 56-61.

Chen, L., and Bai, B. (2013). "Equilibrium, kinetic, thermodynamic, and in situ regeneration studies about methylene blue adsorption by the raspberry-like TiO2@ yeast microspheres." Industrial & Engineering Chemistry Research, 52(44), 15568-15577.

Deng, H., Lu, J., Li, G., Zhang, G., and Wang, X. (2011). "Adsorption of methylene blue on adsorbent materials produced from cotton stalk." Chemical Engineering Journal, 172(1), 326-334.

Elsagh, A., Moradi, O., Fakhri, A., Najafi, F., Alizadeh, R., and Haddadi, V. (2017). "Evaluation of the potential cationic dye removal using adsorption by graphene and carbon nanotubes as adsorbents surfaces." Arabian Journal of Chemistry, 10, S2862-S2869.

Ezzeddine, Z., Batonneau-Gener, I., Pouilloux, Y., and Hamad, H. (2016). "Removal of methylene blue by mesoporous CMK-3: Kinetics, isotherms and thermodynamics." Journal of Molecular Liquids, 223(Supplement C), 763-770.

Gromov, D. G., Bulyarskii, S., Pavlov, A., Scorik, S., Shulyat'ev, A., and Trifonov, A. Y. (2016). "Catalytic CVD-growth of array of multiwall carbon nanotubes on initially amorphous film Co–Zr–N–O." Diamond and Related Materials, 64(Supplement C), 97-102.

Hu, C., Lin, Y., Connell, J. W., Cheng, H. M., Gogotsi, Y., Titirici, M. M., and Dai, L. (2019). "Carbon-Based Metal-Free Catalysts for Energy Storage and Environmental Remediation." Advanced Materials, 31(13), 1806128.

Jeong, S., Lee, J., Kim, H.-C., Hwang, J. Y., Ku, B.-C., Zakharov, D. N., Maruyama, B., Stach, E. A., and Kim, S. M. (2016). "Direct observation of morphological evolution of a catalyst during carbon nanotube forest growth: new insights into growth and growth termination." Nanoscale, 8(4),

2055-2062.

Li, Y.-h., Gao, H.-q., Yang, J.-h., Gao, W.-l., Xiang, J., and Li, Q.-y. (2014). "Multi-wall carbon nanotubes supported on carbon fiber paper synthesized by simple chemical vapor deposition." Materials Science and Engineering: B, 187, 113-119.

Liu, Y., Kang, Y., Mu, B., and Wang, A. (2014). "Attapulgite/bentonite interactions for methylene blue adsorption characteristics from aqueous solution." Chemical Engineering Journal, 237, 403-410.

Meshot, E. R., Zwissler, D. W., Bui, N., Kuykendall, T. R., Wang, C., Hexemer, A., Wu, K. J. J., and Fornasiero, F. (2017). "Quantifying the Hierarchical Order in Self-Aligned Carbon Nanotubes from Atomic to Micrometer Scale." ACS nano.

Norzilah, A., Fakhru'l-Razi, A., Choong, T. S., and Chuah, A. L. (2011). "Surface modification effects on CNTs adsorption of methylene blue and phenol." Journal of Nanomaterials, 2011, 55.

Shen, K., Chen, X., Chen, J., and Li, Y. (2016). "Development of MOF-derived carbon-based nanomaterials for efficient catalysis." ACS Catalysis, 6(9), 5887-5903.

Siddiqui, S. I., Fatima, B., Tara, N., Rathi, G., and Chaudhry, S. A. (2019). "Recent advances in remediation of synthetic dyes from wastewaters using sustainable and low-cost adsorbents." The Impact and Prospects of Green Chemistry for Textile Technology, Elsevier, 471-507.

Subramani, S., and Thinakaran, N. (2017). "Isotherm, kinetic and thermodynamic studies on the adsorption behaviour of textile dyes onto chitosan." Process Safety and Environmental Protection, 106, 1-10.

Sun, D. L., Hong, R. Y., Liu, J. Y., Wang, F., and Wang, Y. F. (2016). "Preparation of carbon nanomaterials using two-group arc discharge plasma." Chemical Engineering Journal, 303, 217-230.

Suresh, S., Sugumar, R. W., and Maiyalagan, T. (2011). "Equilibrium and Kinetic studies on the adsorption of Methylene blue from aqueous solution onto activated carbon prepared from Murraya koenigii (curry tree) stems." Asian Journal of Chemistry, 23(10), 4486.

Tao, F., and Crozier, P. A. (2016). "Atomic-scale observations of catalyst structures under reaction conditions and during catalysis." Chemical reviews, 116(6), 3487-3539.

Wang, C., Yang, S., Ma, Q., Jia, X., and Ma, P.-C. (2017). "Preparation of carbon nanotubes/graphene hybrid aerogel and its application for the adsorption of organic compounds." Carbon, 118, 765-771.

Wang, J., Chen, Z., and Chen, B. (2014). "Adsorption of polycyclic aromatic hydrocarbons by graphene and graphene oxide nanosheets." Environmental science & technology, 48(9), 4817-4825.

Wang, S., Ng, C. W., Wang, W., Li, Q., and Hao, Z. (2012). "Synergistic and competitive adsorption of organic dyes on multiwalled carbon nanotubes." Chemical engineering journal, 197, 34-40.

Xiong, L., Yang, Y., Mai, J., Sun, W., Zhang, C., Wei, D., Chen, Q., and Ni, J. (2010). "Adsorption behavior of methylene blue onto titanate nanotubes." Chemical Engineering Journal, 156(2), 313-320.

Zhou, L., Ji, L., Ma, P.-C., Shao, Y., Zhang, H., Gao, W., and Li, Y. (2014). "Development of carbon nanotubes/CoFe 2 O 4 magnetic hybrid material for removal of tetrabromobisphenol A and Pb (II)." Journal of hazardous materials, 265, 104-114.

Zohre, S., Ataallah, S. G., and Mehdi, A. (2010). "Experimental study of methylene blue adsorption from aqueous solutions onto carbon nano tubes." International Journal of Water Resources and Environmental Engineering, 2 (2), 016 -028.